analytical chemistry

pubs.acs.org/ac Article

Pushing OECTs toward Wearable: Development of a Miniaturized Analytical Control Unit for Wireless Device Characterization

Xinyu Tian,[‖] Dingyao Liu,[‖] Jing Bai, Kai San Chan, Long Ching Ip, Paddy K. L. Chan, and Shiming Zhang*

Cite This: *Anal. Chem.* 2022, 94, 6156−6162 Read Online

ACCESS | Metrics & More | Article Recommendations | Supporting Information

ABSTRACT: Organic electrochemical transistors (OECTs) have emerged as a next-generation biosensing technology because of their water-stability, cost-effectiveness, and ability to obtain high sensitivity at low operation voltage (mV). However, a miniaturized readout unit that can wirelessly characterize the overall performance of an OECT is still missing, which hinders the assembling of truly wearable OECT systems for continuous health-monitoring applications. In this work, we present a coin-sized analytical unit for remote and wireless OECT characterization, namely, a personalized electronic reader for electrochemical transistors (PERfECT). It has been verified that PERfECT can measure the transfer, output, hysteresis, and transient behavior of OECTs with resolution and sampling rate on par with the bulky equipment used in laboratories. PERfECT is also capable of characterizing other low-voltage transistors. An integrated board for multiplexed OECT characterizations (32 channels) has also been demonstrated. This work provides a missing building block for developing next-generation OECT-based bioelectronics for digital wearable applications.

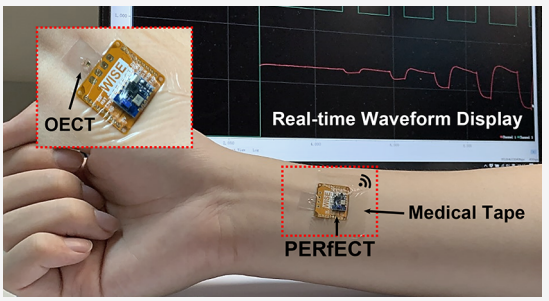

Portable and wearable biosensors are heavily researched nowadays to achieve the goal of decentralized and personalized healthcare.[1−7] Organic electrochemical transistors (OECTs), which combine the advantages of both an electrochemical cell and a microelectronic transistor, have a high signal-amplification ability and are energy-efficient.[8−12] The conventional OECT device structure is illustrated in Figure 1. It consists of source and drain electrodes, an organic semiconductor channel, an electrolyte, and a gate electrode. The organic semiconductor channel, for example, poly(3,4-ethylenedioxythiophene) polystyrenesulfonate (PEDOT:PSS), is in direct contact with the electrolyte in which the gate electrode is immersed. When a positive (negative) gate voltage (V_{gs}) is applied, the cations (anions) in the electrolyte are electrostatically repulsed into the channel, and an electrochemical dedoping (doping) process subsequently occurs. This dedoping (doping) process changes the conductivity of the channel. In this way, a slight change in V_{gs} is converted to a large change in the source-drain current (I_{ds}), which leads to a high transconductance (G_m).[13] Therefore, OECTs have been widely explored for applications in health monitoring,[14−20] bioelectronic interfacing,[21−24] and neuromorphic computing.[25−27] However, despite these advances, a miniaturized and wireless OECT characterization system is still missing, which is an indispensable building block to developing truly integrated OECTs for continuous healthcare monitoring applications. The development of such a wearable OECT characterization system is challenging because it requires transdisciplinary effort among analytical chemistry, electrochemistry, microelectronics, embedded system and wireless communication.

In this work, we report a coin-sized analytical unit, namely, a personalized electronic reader for electrochemical transistors (PERfECT), for wireless OECT characterization. The PERfECT system is developed by a strategic integration of state-of-the-art electronic analytical units and software engineering. Systematic work is conducted to tailor the analytical features of PERfECT to meet the specific requirements for OECT characterization. In addition to OECTs, PERfECT is also capable of characterizing other kinds of low-voltage transistors. Significantly, the figure of merit of PERfECT is on par with the bulky equipment used in laboratories. These merits make PERfECT a highly pursued analytical unit for the development of next-generation medical wearables with advanced low voltage transistor technologies.

EXPERIMENTAL SECTION

Fabrication of OECT. OECTs were fabricated on stretchable substrates (3M Tegaderm roll). The source, drain, and gate electrodes were prepatterned on the stretchable

Received: December 1, 2021
Accepted: March 27, 2022
Published: April 6, 2022

https://doi.org/10.1021/acs.analchem.1c05210
Anal. Chem. 2022, 94, 6156−6162

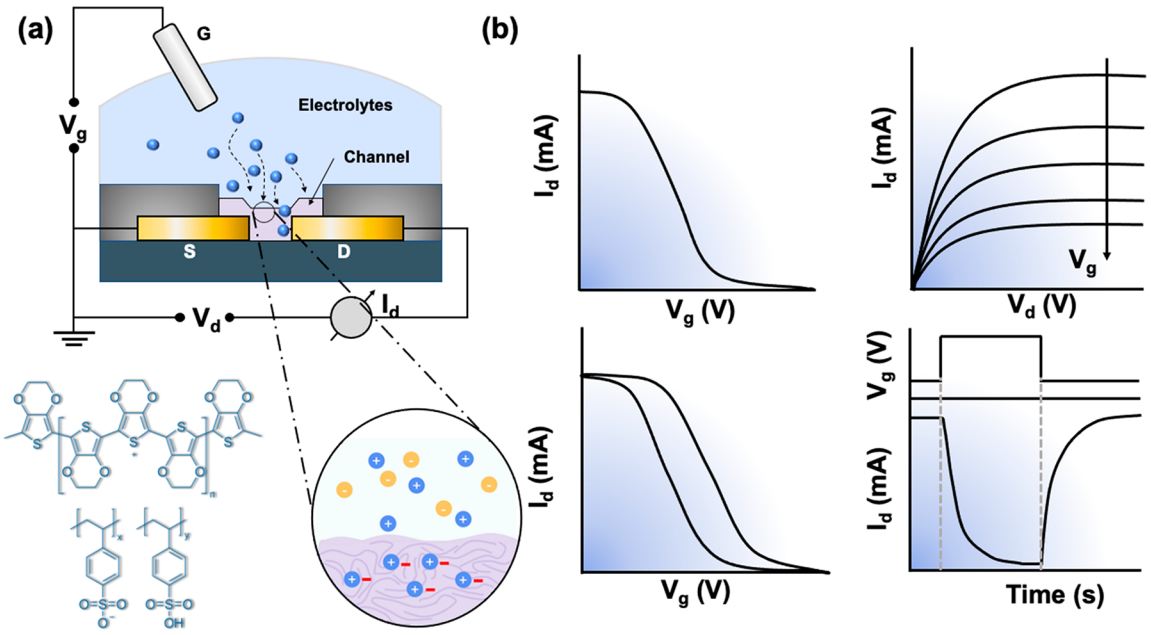

Figure 1. Typical structure of an OECT and its characterization methods. (a) Schematic diagram of the device structure of an OECT. (b) Typical characterizations of OECT: transfer curve, output curve, hysteresis loop, and transient response.

substrate in a planar structure. Then, a PEDOT:PSS suspension was spin-coated and patterned between the source and drain electrodes. Kapton tape was used as a shadow mask for patterning of the channel. Prior to spin-coating, the PEDOT:PSS suspension was mixed with surfactant dodecyl benzenesulfonic acid (DBSA) (0.5 v/v %) and cross-linker 3-glycidoxypropyltrimethoxysilane (GOPS) (1 v/v %) to improve the wettability and adhesion to the substrate. The sample was then baked on a hot plate for 1 h to anneal the PEDOT:PSS channel. Afterward, devices were soaked in deionized water to remove saline contaminants from the PEDOT:PSS film. A solid-state ion gel was subsequently used as an electrolyte bridging the gate electrode and the PEDOT:PSS channel. Note that the ion gel was prepared through one-step polymerization in which zwitterionic monomer 3-dimethyl(methacryloyloxyethyl) ammonium propanesulfonate (DMAPS) was first mixed with an ionic liquid (1-ethyl-3-methylimidazolium ethyl sulfate) and deionized water in a weight ratio of 1:1:4.67 and then initialized by ammonium persulfate (APS) at 70 °C for 6 h. After curing in a 50 °C oven to remove excess water, the ion gel was obtained. OECT characterization was performed with both a PERfECT analytical unit and commercial equipment (Agilent Keithley B2902A).

Fabrication of PERfECT. Figure 2 shows the assembled PERfECT analytical unit for OECT characterization. The circuit diagram of PERfECT was designed with open-source electronic design automation software. The flexible printed circuit board (fPCB) of PERfECT was manufactured by a commercial PCB manufacturer (JDBPCB) (details in Figure S1). All of these electronic and analytical components were ordered from DigiKey (USA) and were subsequently integrated into the fPCB board. The customized assembly of these units was conducted in collaboration with the SESIC Co., Limited. The circuit was programmed with the Joint Test Action Group (JTAG) interface, and the circuit's firmware was developed with C language. Multilayer manufacturing processes were used to scale down the dimension of the fPCB board for wearable applications.

RESULTS AND DISCUSSION

Development of PERfECT. The development of PERfECT started with the functional design and optimal combination of tiny electronic analytical components that can accurately control the source voltage (V_s), drain voltage (V_d), and gate voltage (V_g) (Figure 2). Therefore, it can measure the corresponding I_{ds} with the highest possible resolution.

For wearable OECT characterization, it is critically required that (i) both the source-drain voltage (V_{ds}) and V_{gs} can be swept from −1 to +1 V at high resolution (<1 mV/step) and a high sweeping speed (<1 ms/step); (ii) I_{ds} ranging from nA to mA is measurable, with a high resolution (<1 nA); (iii) the I_{ds} sampling rate should be as fast as possible (>10 KSPS); and (iv) the physical size of the PERfECT system is smartwatch-compatible so that it can be better integrated with commercial electronics for practical wearable applications.

To simultaneously satisfy all of the above requirements, four analytical modules were used and integrated into the PERfECT system: (i) A potential output control module that contains three digital-to-analog converters (DAC) and negative feedback network-based potentiostat amplifiers to control V_s, V_d, and V_g (details in Figure S2). High-speed 12-bit DACs were used to control the output voltage, which leads to a high resolution of <1 mV/step and a fast sweeping speed of <1 ms/step. (ii) A high-accuracy current monitor module which contains a trans-impedance amplifier (TIA) and an analog-to-digital converter (ADC). The TIA was used to control the output voltage and convert the input I_{ds} to a voltage value. A 16-bit ADC was used to increase the I_{ds} readout resolution (<1 nA). (iii) A microcontroller unit (MCU) controlling the working sequences of DAC, TIA, and ADC for specific functions. (iv) A wireless communication module for data exchange and transmission with mobiles. Additionally, an internal temperature sensor was embedded for

https://doi.org/10.1021/acs.analchem.1c05210
Anal. Chem. 2022, 94, 6156−6162

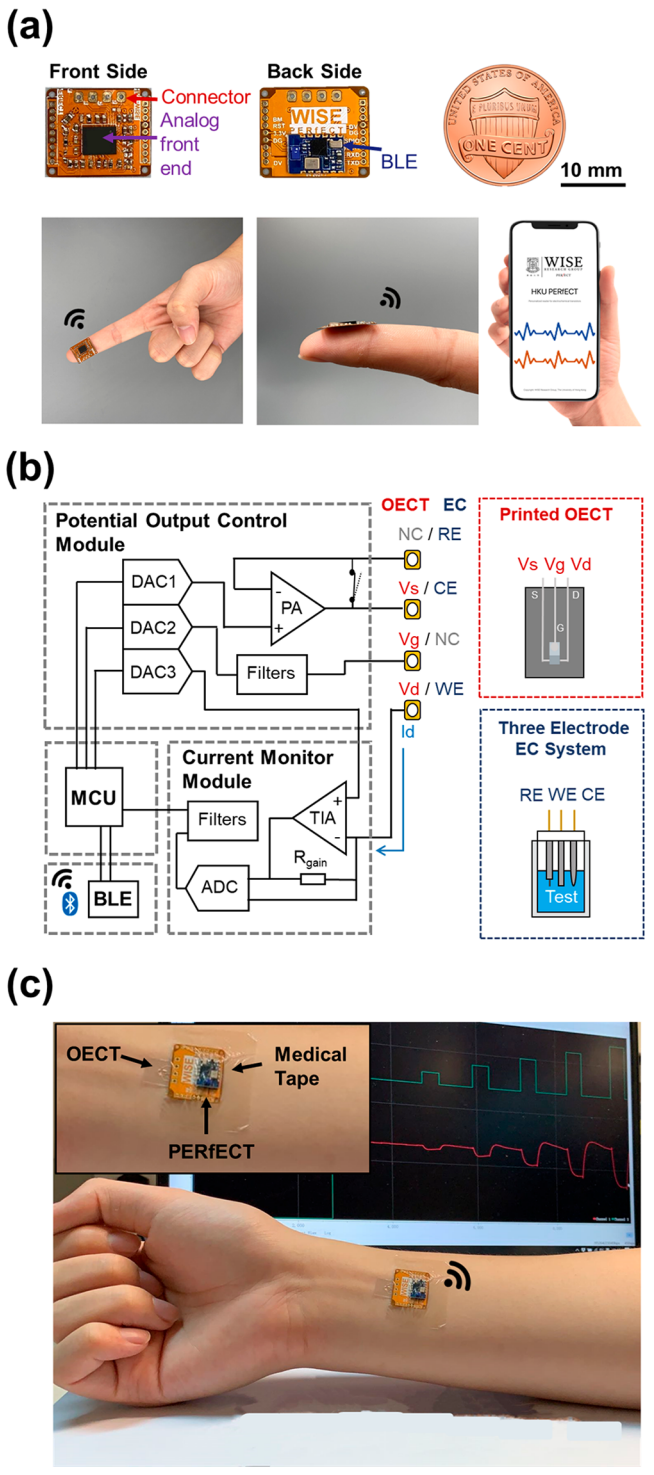

Figure 2. Design of the PERfECT system. (a) Optical images of the PERfECT system. The OECT or EC sensors are plugged into the connector and measured by the analog front end. A host APP in the smartphone: i) controls the experimental protocol; ii) processes, visualizes, and stores the data; and iii) transmits it to the cloud. (b) Circuit diagram and main components of PERfECT. (c) Demonstration of the use of PERfECT for wearable applications.

real-time temperature recording and data calibration (details in Figure S3). After a strategic integration of the above components, the dimension of PERfECT was successfully scaled down to less than 1.5 cm × 1.5 cm, an ideal size for wearable uses.

The self-calibration of OECTs is desired for reliable signal recording because performance degradation occurs in practical biosensing applications.[28] However, previously reported OECT-based biosensing circuits cannot be self-calibrated because they are not able to dynamically control V_{ds}.[15,20,29] This technical challenge is addressed in the PERfECT system by using an additional potential control module to separately control V_d and V_s. Therefore, the OECT can be calibrated on demand, which can potentially promote its use for practical applications. Moreover, the PERfECT system can also be converted to a miniaturized electrochemical (EC) station[30] because of the integrated potentiostat amplifier (PA) analytical unit, which can help to set the reference electrode.[30] When used in EC mode, the source electrode and the drain electrode of OECTs serve as working and counter electrodes (Supporting Information Figure S4). Therefore, PERfECT can be used in both EC mode and OECT mode, which is advantageous for data verification and device calibration.

OECT Characterization with PERfECT. The accuracy and reliability of PERfECT in characterizing OECTs were evaluated by measuring the following four typical curves: (i) transfer curve, (ii) output curve, (iii) hysteresis curve, and (iv) transient response curve (shown in Figure 1(c–f)).

Transfer Curve. The transfer curve indicates the change in I_{ds} (i.e., doping level evolution of the channel) with V_{gs}. It can be used to extract secondary performance indicators of the OECTs such as the on/off ratio and the G_m at different V_{gs} values.[31] For transfer characterization of OECTs, V_{ds} is fixed at a constant value. V_{gs} is scanned normally between −1 and +1 V. In most cases, V_{gs} is set to less than ±1.23 V to avoid water hydrolysis.[15]

Figure 3a compares the transfer curves of an OECT measured by PERfECT and by a commercial source measure unit (SMU). Identical curves were obtained, demonstrating the high reliability of the PERfECT system. To further evaluate the capability of PERfECT in detecting ultralow current (~nA), we subsequently investigated the transfer profile at higher V_{gs} (0.8 V). The result indicated that PERfECT can measure I_{ds} with a high resolution of down to 1 nA (Figure 3a, inset). Figure 3b shows the transconductance value extracted from the transfer curves measured by PERfECT and SMU. Identical transconductance profiles were obtained over a wide range of V_{gs} (0–0.8 V) because of the high resolution of PERfECT.

Output Curve. The output curve indicates the relationship between I_{ds} and V_{ds} at a constant V_{gs}.[32] It is used to investigate the working mode of OECT (linear or saturation) and the associated amplification potential for biosensing applications. To obtain a high-quality output curve, the resolution of V_{ds} should be as high as possible. To satisfy this requirement, PERfECT is designed that can control V_{ds} with a resolution of less than 1 mV (Figure 2b).

Figure 3c compares the output curves of OECT measured by both PERfECT and SMU. Benefited from PERfECT's high resolution in controlling V_{ds} as well as the accuracy in recording I_{ds}, the output curve measured by PERfECT showed a great match to that obtained by SMU. For example, the I_{ds} difference between PERfECT and SMU is less than ±1%, regardless of V_{gs}. The ±1% measurement error is attributed to the difference in contact resistance. To further validate this hypothesis, we replaced the channel with a commercial resistor whose resistance value is fixed (400 Ω). As shown in the Supporting Information (Figure S5), in this two-terminal device (no V_{gs}), the slope of the curve indicates the resistance

https://doi.org/10.1021/acs.analchem.1c05210
Anal. Chem. 2022, 94, 6156−6162

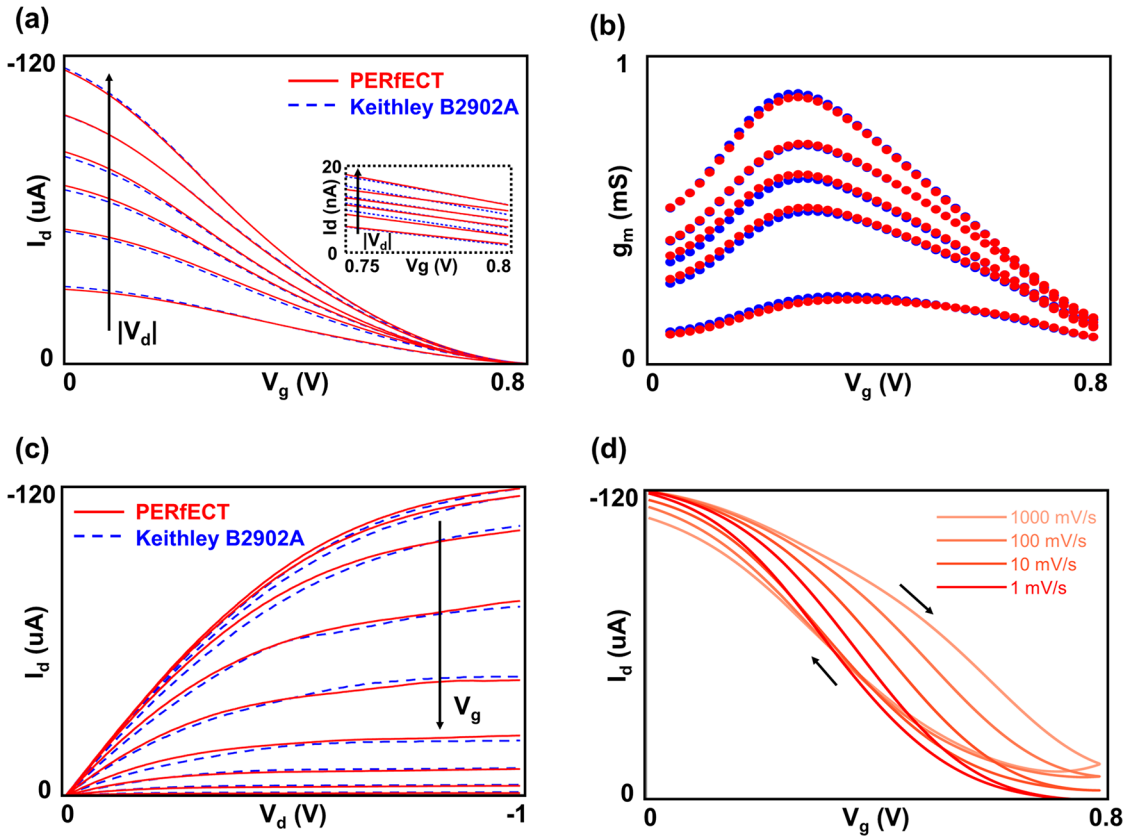

Figure 3. Characterization of OECTs with PERfECT. (a) Transfer curves. For both PERfECT and SMU, V_g was scanned between −0.2 and 0.8 V and V_d was fixed in each curve. The V_g scan step was configured at 5 mV, and each step had a 1.5 S interval. V_d was changed from −0.1 to −0.6 V after finishing the V_g scan. (b) Related transconductance. (c) Output characterization, in which the V_d scan step was 5 mV and V_g was changed from 0 to 0.8 V in a step of 100 mV. (d) Hysteresis characterization by the PERfECT system. Hysteresis curves with different scan rates of 1, 10, 100, and 1000 mV/s at V_{ds} = −0.6 V were investigated. V_g was changed from 0 to 0.8 V in a step of 5 mV.

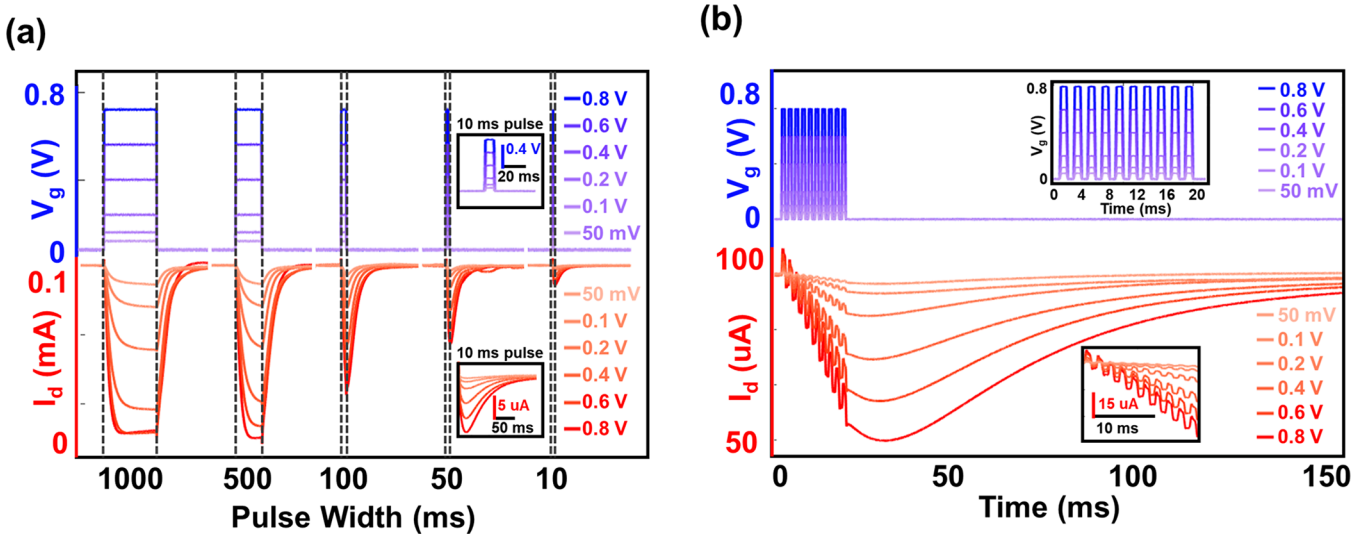

Figure 4. Transient characterization. (a) Current responses (red curves) under different gate pulses (blue curves). The pulse width changed from 10 to 1000 ms, and the amplitude changed from 50 to 800 mV. (b) OECT current responses under a group of 1 ms pulses. The pulse amplitude changed from 50 to 800 mV.

value of the resistor. We observed that PERfECT and SMU showed exactly the same slope, demonstrating the accuracy and high reliability of PERfECT in controlling V_{ds} and monitoring I_{ds}.

Hysteresis Curve. Hysteresis curves of OECTs can help in investigating the dynamic behavior of the device, including the ion diffusion dynamics and the doping kinetics of the channel. However, hysteresis characterization poses an addition requirement that both the sweeping rate and the scanning

https://doi.org/10.1021/acs.analchem.1c05210
Anal. Chem. 2022, 94, 6156−6162

direction of V_{gs} should be controllable, and a high sweeping resolution should be maintained at the same time. PERfECT is specifically designed to meet this requirement. The embedded MCU controls the sweeping directions of the DAC for bidirectional characterization. The high resolution of the DAC permits the high sweeping resolution (less than 0.5 mV). Figure 3d shows the hysteresis curves of OECTs measured with PERfECT, where V_{gs} was controlled over a typical range (−0.2 to 0.8 V) with both a positive and a negative scan. Hysteresis curves with different scan rates of 1, 10, 100, and 1000 mV/s were measured. A larger hysteresis loop was observed at a higher scanning rates, consistent with the results reported previously,[31] and can be attributed to the suppressed doping/dedoping of the channel at higher scanning rates.

Transient Curve. The transient curve of OECT measures the I_{ds} response profile when a V_{gs} pulse is applied or removed. It is used to benchmark the response speed and frequency response of an OECT.[33] Transient characterization is also widely used for evaluating an OECT's synaptic behavior, which is an emerging research topic for brain-inspired neuromorphic computing applications.[25−27,34] However, despite the importance of the transient behavior of OECTs, its characterization is challenging simply because it requires accurate control of V_{gs}, the pulse width and pulse amplitude. In addition, the duty time, the period, the rest time,[26] and the delay time should be simultaneously controlled precisely to realize a full-spectrum measurement of the transient behavior.

To fulfill the above-mentioned critical requirements, we further incorporated a programmable analytical pulse waveform generation function into PERfECT without increasing the physical size of the whole system. The updated system allows the generation of a high-profile pulses (with a pulse width down to 1 ms and a pulse amplitude controllable between 0.6 mV and 1.5 V). To facilitate operation, we further designed a user-friendly interface that allows the customization of the pulse profiles. As shown in Figure 4, PERfECT can output precise pulses where both the pulse width (Figure 4a) and pulse amplitude (Figure 6 inset) can be accurately controlled. The I_{ds} responded rapidly to the change of the pulses, and expected profiles were recorded (Video S1). To validate the potential of PERfECT for the characterization of the transient behavior of OECTs, we investigated OECT's synaptic behavior by recording the I_{ds} at given pulse trains[26] (Figure 4b). The I_{ds} showed a distinct decrease with increased pulse numbers. The increase in pulse amplitude led to a steeper I_{ds} decrease. These results demonstrate that the PERfECT system has the full capability to characterize the neuromorphic behavior of OECTs, encouraging their uses for the rising brain-inspired neuromorphic computing and wearable edge-computing applications.

PERfECT Prototype for Wearable Biosensing. Finally, to show the capability of PERfECT for practical applications, we demonstrated a fully integrated wearable biosensor prototype where PERfECT, an OECT sensor, and a reference EC electrode were embedded together in a watch (Figure S6). Platinum was used as the gate electrode of the OECT for the detection of hydrogen peroxide (H_2O_2). As shown in Figure 5a, PERfECT could transmit a stable I_{ds} of the OECT sensor and a stable amperometric current of an EC sensor to the mobile. The OECT sensor showed a high sensitivity (slope in Figure 5b). The sensor was reusable and remained functional after 1 month's use because of the excellent air and water stability of OECTs.

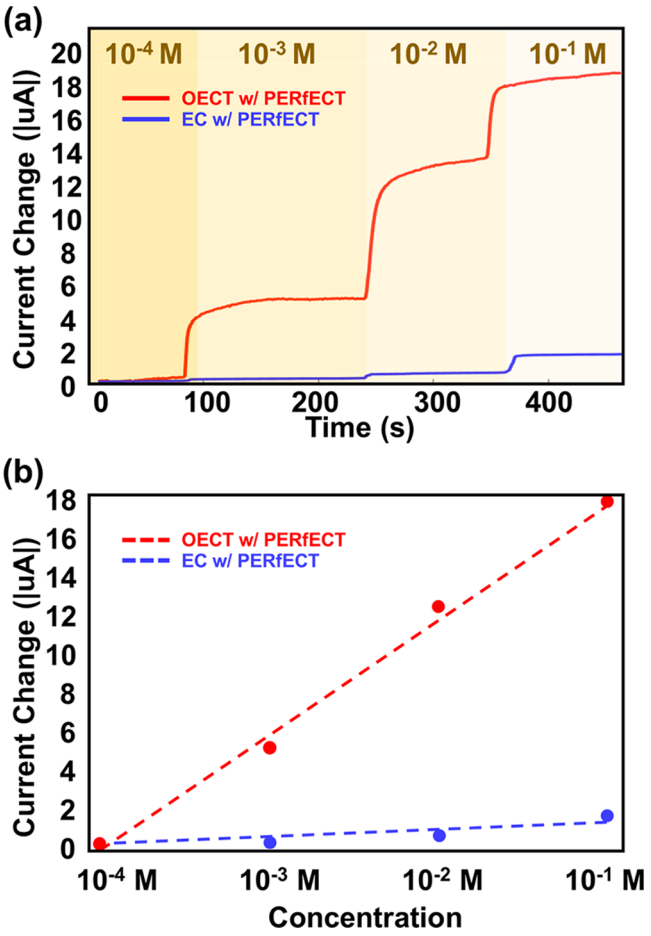

Figure 5. PERfECT-based prototype for wearable biosensing applications. Detection of hydrogen peroxide with an EC electrode and with an OECT, both were measured wirelessly with the PERfECT platform.

CONCLUSIONS

We have reported a coin-sized analytical control unit, PERfECT, for wireless OECT characterization. The PERfECT system can precisely characterize the transfer curve, output curve, hysteresis loop, and transient response of an OECT. The figure of merit of PERfECT is on par with that of a commercial bulky equipment. For example, the I_{ds} readout resolution is as low as 1 nA. The data sampling rate is as high as 200 KSPS. These unique properties make the PERfECT system capable of continuously recoding of subtle signals, which paves the way for using OECTs for wearable and personalized sensing applications.

The PERfECT system can also serve as a miniaturized electrochemical station for wearable EC measurements. The scanning rate can be controlled between 1 and 1000 mV/s. This added function permits a facile route to calibrating the OECT biosensors, making the whole system competitive for more complicated biosensing applications.

Although the PERfECT system presented here is for OECT characterizations, it has the full capability to measure other kinds of low-voltage transistors such as electrolyte-gated field-effect transistors (FETs) and high-k dielectric-gated thin-film transistors (both FETs and ECTs). Therefore, the PERfECT platform allows the immediate development of other wearable systems based on low-voltage transistors. In particular, we envision PERfECT(s) will significantly promote the research

https://doi.org/10.1021/acs.analchem.1c05210
Anal. Chem. 2022, 94, 6156−6162

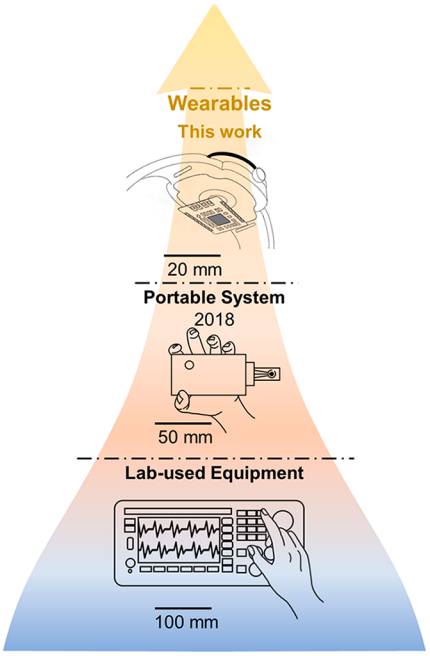

	Keithley 2902B	CHI600E	2018 [30]	2020 [20]	PERfECT This work
Vds measure	**Yes**	N/A	N/A	Yes	**Yes**
Vgs control	**Yes**	N/A	N/A	Yes	**Yes**
Vds control	**Yes**	N/A	N/A	N/A	**Yes**
Transfer curve	**Yes**	N/A	N/A	N/A	**Yes**
Output curve	**Yes**	N/A	N/A	N/A	**Yes**
Transient curve	**Yes**	N/A	N/A	N/A	**Yes**
Hysteresis curve	**Yes**	N/A	N/A	N/A	**Yes**
CV	N/A	**Yes**	**Yes**	N/A	**Yes**
EIS	N/A	**Yes**	**Yes**	N/A	**Yes**
Flexible	N/A	N/A	N/A	N/A	**Yes**
Size (L * W * H cm)	56 * 21 * 9	37 * 23 * 12	8 * 4 * 2.3	4*2.5*2.5	1.8 * 1.8 * 0.5
Applied dynamic voltage range	200 V	20 V	3 V	3.3 V	2.2 V
Current input range	±10 A	±350 mA	±0.18 mA	N/A	±1.7 mA
Min applied potential step	0.1 uV	0.015 uV	67uV	N/A	0.5 mV
Min current resolution	0.1 fA	0.3fA	6.4 nA	N/A	1 nA
Sampling rate	20K SPS	1M SPS	<1K SPS	2K SPS	200K SPS
Power consumption	200 W	N/A	~ 0.02 W	N/A	~ 0.02 W

Figure 6. Comparison between this work and the previously reported EC/ECT readout systems. PERfECT is the first platform that allows the development of smartwatch-compatible and wearable OECT-based biosensors with resolution on par with the bulky equipment used in laboratories. In addition, PERfECT can be powered simply with a button cell (Figure S7). An integrated board for multiplexed OECT characterization (32 channels) has also been developed based on one PERfECT unit (Figure S8), promoting the use of low-voltage transistors for developing e-skins, microelectrode arrays (MEAs), high-density transistor-based neuron probes and neuromorphic hardware. N/A means not available.

of developing wearable edge-computing hardware,[35,36] where sensing, data storage, and computing can be realized in a miniaturized wearable entity.

■ ASSOCIATED CONTENT

Supporting Information

The Supporting Information is available free of charge at https://pubs.acs.org/doi/10.1021/acs.analchem.1c05210.

Additional experimental details including real-time temperature monitoring, current recording accuracy, cyclic voltammetry measurements, a wearable demonstration, and the calculation of power consumption (PDF)

Demonstration of using PERfECT as a wearable platform to characterize a skin-attachable OECT device (MP4)

■ AUTHOR INFORMATION

Corresponding Author

Shiming Zhang − *Department of Electrical and Electronic Engineering, The University of Hong Kong, Hong Kong SAR, China*; Email: szhang@eee.hku.hk

Authors

Xinyu Tian − *Department of Electrical and Electronic Engineering, The University of Hong Kong, Hong Kong SAR, China*

Dingyao Liu − *Department of Electrical and Electronic Engineering, The University of Hong Kong, Hong Kong SAR, China*

Jing Bai − *Department of Electrical and Electronic Engineering, The University of Hong Kong, Hong Kong SAR, China*

Kai San Chan − *Biomedical Engineering Program, The University of Hong Kong, Hong Kong SAR, China*

Long Ching Ip − *Biomedical Engineering Program, The University of Hong Kong, Hong Kong SAR, China*

Paddy K. L. Chan − *Department of Mechanical Engineering, The University of Hong Kong, Hong Kong SAR, China*; orcid.org/0000-0002-3166-2192

Complete contact information is available at: https://pubs.acs.org/10.1021/acs.analchem.1c05210

Author Contributions

‖X.T. and D.L. contributed equally.

Notes

The authors declare no competing financial interest.

■ ACKNOWLEDGMENTS

S.Z. acknowledges startup funds from the University of Hong Kong and the Innovation Wing Two Research Fund from the Tam Wing Fan Innovation Wing for supporting this work.

■ REFERENCES

(1) Kim, J.; Campbell, A. S.; De Ávila, B. E.-F.; Wang, J. *Nat. Biotechnol.* **2019**, *37*, 389−406.

(2) Gao, W.; Emaminejad, S.; Nyein, H. Y. Y.; Challa, S.; Chen, K.; Peck, A.; Fahad, H. M.; Ota, H.; Shiraki, H.; Kiriya, D. *Nature.* **2016**, *529*, 509−514.

(3) Rose, D. P.; Ratterman, M. E.; Griffin, D. K.; Hou, L.; Kelley-Loughnane, N.; Naik, R. R.; Hagen, J. A.; Papautsky, I.; Heikenfeld, J. C. *IEEE Trans. Biomed. Eng.* **2015**, *62*, 1457−1465.

(4) Zhou, Z.; Chen, K.; Li, X.; Zhang, S.; Wu, Y.; Zhou, Y.; Meng, K.; Sun, C.; He, Q.; Fan, W. *Nat. Electron.* **2020**, *3*, 571−578.

(5) Zhou, Y.; Zhao, X.; Xu, J.; Fang, Y.; Chen, G.; Song, Y.; Li, S.; Chen, J. *Nat. Mater.* **2021**, *20*, 1670−1676.

https://doi.org/10.1021/acs.analchem.1c05210
Anal. Chem. 2022, 94, 6156−6162

(6) Zhao, X.; Zhou, Y.; Xu, J.; Chen, G.; Fang, Y.; Tat, T.; Xiao, X.; Song, Y.; Li, S.; Chen, J. *Nat. Commun.* **2021**, *12*, 6755.
(7) Chen, G.; Xiao, X.; Zhao, X.; Tat, T.; Bick, M.; Chen, J. *Chem. Rev.* **2022**, *122*, 3259−3291.
(8) Rivnay, J.; Inal, S.; Salleo, A.; Owens, R. M.; Berggren, M.; Malliaras, G. G. *Nat. Commun.* **2018**, *3*, 17086.
(9) Zhang, S.; Hubis, E.; Girard, C.; Kumar, P.; Defranco, J.; Cicoira, F. *J. Mater. Chem. C* **2016**, *4*, 1382−1385.
(10) Zhang, L.; Wang, G.; Wu, D.; Xiong, C.; Zheng, L.; Ding, Y.; Lu, H.; Zhang, G.; Qiu, L. *Biosens. Bioelectron.* **2018**, *100*, 235−241.
(11) Wu, X.; Surendran, A.; Moser, M.; Chen, S.; Muhammad, B. T.; Maria, I. P.; McCulloch, I.; Leong, W. L. *ACS Appl. Mater. Interfaces.* **2020**, *12*, 20757−20764.
(12) Guo, X.; Cao, Q.; Liu, Y.; He, T.; Liu, J.; Huang, S.; Tang, H.; Ma, M. *Anal. Chem.* **2020**, *92*, 908−915.
(13) Khodagholy, D.; Rivnay, J.; Sessolo, M.; Gurfinkel, M.; Leleux, P.; Jimison, L. H.; Stavrinidou, E.; Herve, T.; Sanaur, S.; Owens, R. M.; Malliaras, G. G. *Nat. Commun.* **2013**, *4*, 2133.
(14) Liu, H.; Zhang, S.; Li, Z.; Lu, T. J.; Lin, H.; Zhu, Y.; Ahadian, S.; Emaminejad, S.; Dokmeci, M. R.; Xu, F.; Khademhosseini, A. *Matter* **2021**, *4*, 2886.
(15) Braendlein, M.; Lonjaret, T.; Leleux, P.; Badier, J.-M.; Malliaras, G. G. *Advanced Science* **2017**, *4*, 1600247.
(16) Bai, L.; Elósegui, C. G.; Li, W.; Yu, P.; Fei, J.; Mao, L. *Front. Chem.* **2019**, *7*, DOI: 10.3389/fchem.2019.00313.
(17) Tyrrell, J. E.; Boutelle, M. G.; Campbell, A. J. *Adv. Funct. Mater.* **2021**, *31*, 2007086.
(18) Liu, H.; Yang, A.; Song, J.; Wang, N.; Lam, P.; Li, Y.; Law, H. K.-W.; Yan, F. *Sci. Adv.* **2021**, *7*, DOI: 10.1126/sciadv.abg8387.
(19) Fu, Y.; Wang, N.; Yang, A.; Xu, Z.; Zhang, W.; Liu, H.; Law, H. K.-w.; Yan, F. *Anal. Chem.* **2021**, *93*, 14359.
(20) Zhang, S.; Ling, H.; Chen, Y.; Cui, Q.; Ni, J.; Wang, X.; Hartel, M. C.; Meng, X.; Lee, K.; Lee, J.; Sun, W.; Lin, H.; Emaminejad, S.; Ahadian, S.; Ashammakhi, N.; Dokmeci, M. R.; Khademhosseini, A. *Adv. Funct. Mater.* **2020**, *30*, 1906016.
(21) Khodagholy, D.; Doublet, T.; Quilichini, P.; Gurfinkel, M.; Leleux, P.; Ghestem, A.; Ismailova, E.; Hervé, T.; Sanaur, S.; Bernard, C.; Malliaras, G. G. *Nat. Commun.* **2013**, *4*, 1575.
(22) Keene, S. T.; Fogarty, D.; Cooke, R.; Casadevall, C. D.; Salleo, A.; Parlak, O. *Adv. Adv. Healthcare Mater.* **2019**, *8*, 1901321.
(23) Rivnay, J.; Leleux, P.; Ferro, M.; Sessolo, M.; Williamson, A.; Koutsouras, D. A.; Khodagholy, D.; Ramuz, M.; Strakosas, X.; Owens, R. M.; Benar, C.; Badier, J.-M.; Bernard, C.; Malliaras, G. G. *Sci. Adv.* **2015**, *1*, No. e1400251.
(24) Sim, K.; Ershad, F.; Zhang, Y.; Yang, P.; Shim, H.; Rao, Z.; Lu, Y.; Thukral, A.; Elgalad, A.; Xi, Y. *Nat. Electron.* **2020**, *3*, 775−784.
(25) Van De Burgt, Y.; Lubberman, E.; Fuller, E. J.; Keene, S. T.; Faria, G. C.; Agarwal, S.; Marinella, M. J.; Alec Talin, A.; Salleo, A. *Nat. Mater.* **2017**, *16*, 414−418.
(26) Ji, X.; Paulsen, B. D.; Chik, G. K. K.; Wu, R.; Yin, Y.; Chan, P. K. L.; Rivnay, J. *Nat. Commun.* **2021**, *12*, DOI: 10.1038/s41467-021-22680-5.
(27) Fuller, E. J.; Keene, S. T.; Melianas, A.; Wang, Z.; Agarwal, S.; Li, Y.; Tuchman, Y.; James, C. D.; Marinella, M. J.; Yang, J. J.; Salleo, A.; Talin, A. A. *Science.* **2019**, *364*, 570−574.
(28) Bandodkar, A. J.; Jeerapan, I.; Wang, J. *ACS Sens.* **2016**, *1*, 464−482.
(29) Ji, X.; Lau, H. Y.; Ren, X.; Peng, B.; Zhai, P.; Feng, S.-P.; Chan, P. K. L. *Adv. Mater. Technol.* **2016**, *1*, 1600042.
(30) Ainla, A.; Mousavi, M. P. S.; Tsaloglou, M.-N.; Redston, J.; Bell, J. G.; Fernández-Abedul, M. T.; Whitesides, G. M. *Anal. Chem.* **2018**, *90*, 6240−6246.
(31) Kumar, P.; Yi, Z.; Zhang, S.; Sekar, A.; Soavi, F.; Cicoira, F. *Appl. Phys. Lett.* **2015**, *107*, 053303.
(32) Tybrandt, K.; Zozoulenko, I. V.; Berggren, M. *Sci. Adv.* **2017**, *3*, No. eaao3659.
(33) Rivnay, J.; Ramuz, M.; Leleux, P.; Hama, A.; Huerta, M.; Owens, R. M. *Appl. Phys. Lett.* **2015**, *106*, 043301.
(34) Melianas, A.; Quill, T. J.; Lecroy, G.; Tuchman, Y.; Loo, H. V.; Keene, S. T.; Giovannitti, A.; Lee, H. R.; Maria, I. P.; McCulloch, I.; Salleo, A. *Sci. Adv.* **2020**, *6*, No. eabb2958.
(35) Shim, H.; Sim, K.; Ershad, F.; Yang, P.; Thukral, A.; Rao, Z.; Kim, H.-J.; Liu, Y.; Wang, X.; Gu, G. *Sci. Adv.* **2019**, *5*, No. eaax4961.
(36) Gkoupidenis, P.; Schaefer, N.; Garlan, B.; Malliaras, G. G. *Adv. Mater.* **2015**, *27*, 7176−7180.

https://doi.org/10.1021/acs.analchem.1c05210
Anal. Chem. 2022, 94, 6156−6162